Available online at www.sciencedirect.com

ScienceDirect

Green Energy & Environment 2 (2017) 151−159

www.keaipublishing.com/gee

Research paper

A host-guest approach to fabricate metallic cobalt nanoparticles embedded in silk-derived N-doped carbon fibers for efficient hydrogen evolution

Fenglei Lyu [a], Qingfa Wang [a,**], Han Zhu [b,*], Mingliang Du [b], Li Wang [a], Xiangwen Zhang [a]

[a] Key Laboratory for Green Chemical Technology of the Ministry of Education, School of Chemical Engineering and Technology, Tianjin University, 135 Yaguan Road, Tianjin 300072, China

[b] Department of Materials Engineering, College of Materials and Textiles, Zhejiang Sci-Tech University, Hangzhou 310018, China

Received 5 December 2016; revised 20 January 2017; accepted 28 January 2017
Available online 3 February 2017

Abstract

Hydrogen evolution reaction (HER) plays a key role in generating clean and renewable energy. As the most effective HER electrocatalysts, Pt group catalysts suffer from severe problems such as high price and scarcity. It is highly desirable to design and synthesize sustainable HER electrocatalysts to replace the Pt group catalysts. Due to their low cost, high abundance and high activities, cobalt-incorporated N-doped nanocarbon hybrids are promising candidate electrocatalysts for HER. In this report, we demonstrated a robust and eco-friendly host-guest approach to fabricate metallic cobalt nanoparticles embedded in N-doped carbon fibers derived from natural silk fibers. Benefiting from the one-dimensional nanostructure, the well-dispersed metallic cobalt nanoparticles and the N-doped thin graphitized carbon layer coating, the best Co-based electrocatalyst manifests low overpotential (61 mV@10 mA/cm^2) HER activity that is comparable with commercial 20% Pt/C, and good stability in acid. Our findings provide a novel and unique route to explore high-performance noble-metal-free HER electrocatalysts.

Keywords: Silk; Carbon fibers; Cobalt nanoparticles; Hydrogen evolution; Nitrogen doping

1. Introduction

The energy crisis and environmental concerns caused by the depletion of fossil fuels have stimulated intense research interest in developing renewable energy [1]. Electrochemical water splitting to produce hydrogen is a green technology that can convert renewable energy into a dense mode of energy storage [2]. The conversion efficiencies are often limited by the anode and cathode overpotentials due to the sluggish kinetics caused by multiple-electron transfer [3]. The hydrogen evolution reaction (HER), a cathode reaction, plays a key role in electrochemical water splitting. High efficient electrocatalysts can minimize the overpotential for HER and increase the conversion efficiency. Although platinum is the most effective HER electrocatalyst to date, its high price and scarcity hinder its wide application in water splitting. Therefore, developing HER electrocatalysts with high efficiencies and low prices is of urgent demand [4,5].

Over the past few years, researchers have been dedicated to developing transition-metal and metal-free electrocatalysts as alternatives to Pt for HER [6−17]. Cobalt-based nanomaterials such as chalcogenides [18−22] and phosphides [23−26] have been reported to be efficient HER electrocatalysts. In particular, metallic cobalt incorporated with N-doped nanocarbon hybrids [27−29] have been demonstrated to be promising candidates for HER due to their low cost, high abundance and high activities in both acidic and basic conditions. For example, Zou et al. reported the synthesis of cobalt-embedded

* Corresponding author.
** Corresponding author.
E-mail addresses: qfwang@tju.edu.cn (Q. Wang), zhuhanfj@zstu.edu.cn (H. Zhu).

http://dx.doi.org/10.1016/j.gee.2017.01.007

nitrogen-rich carbon nanotubes (Co-NRCNTs) derived from dicyandiamide and $CoCl_2$ and showed that the material exhibits high activity towards HER. The Co-NRCNTs can afford 10 mA/cm^2 at an overpotential of 260 mV [30]. Jin et al. reported a cobalt−cobalt oxide/N-doped carbon hybrid (CoOx@CN) derived from melamine and cobalt nitrate. The CoOx@CN exhibited an overpotential of 235 mV to reach 10 mA/cm^2 for HER [31]. Zhang et al. have synthesized self-supported and 3D porous Co−C−N complex bonded carbon fiber foam. It reported that the C and N hybrid coordination derived Co−C−N complex can served as active molecule catalytic center for HER [32]. Toxic organic chemicals such as dicyandiamide and melamine are often applied as nitrogen and carbon sources. However, these chemicals may cause environmental and health issues. Despite tremendous effort in the synthesis of cobalt and N-doped nanocarbon hybrids, it still remains a great challenge to design and engineer cobalt-N-doped nanocarbon hybrids in a robust and eco-friendly manner. It is highly desirable to design and synthesize metallic cobalt nanoparticles embedded in one-dimensional N-doped carbon fibers as an efficient HER electrocatalyst.

Silk fiber, a filamentous natural protein fiber, can serve as an ideal host for coupling transition metal precursors because it has a wealth of polypeptides and a high content of C, N, and O atoms. Meanwhile, cobalt is known to catalyze the crystallization of carbon from various organic compounds. Integrating silk fiber with cobalt can provide a great opportunity in exploring sustainable HER electrocatalysts with high efficiency. Herein, we present a host-guest approach to fabricate metallic cobalt nanoparticles embedded in N-doped carbon fibers (Co@NCFs) as HER electrocatalysts. In contrast to the previously reported methods using toxic chemicals as the nitrogen and carbon sources, we utilize natural silk fiber as the carbon and nitrogen source, which also acts as a host to form one-dimensional nanostructures. The silk fibers possess a large number of nitrogen and oxygen groups, which can couple with the cobalt precursor. After the graphitization process, the metallic cobalt nanoparticles were formed and immobilized on the surfaces of silk-derived N-doped carbon fiber. In addition, with the assistance of metallic cobalt, amorphous carbon can be converted into graphitized carbon, improving the conductivity. The strategy is facile, robust and environmentally benign. Remarkably, the Co@NCFs electrocatalysts manifest high HER activity. The best Co@NCFs-0.8 electrocatalyst can achieve 10 mA/cm^2 at a low overpotential of 61 mV, which is comparable with the commercial 20% Pt/C electrocatalyst.

2. Experimental section

2.1. Preparation of Co@NCFs and NCF

In a typical synthesis, *Bombyx mori* silk cocoons were first washed by deionized water three times. Then, the washed silk cocoons were cut into pieces and immersed into $Co(NO_3)_2$/DMF solution for 24 h at room temperature. After that, the silk cocoons were dried in a vacuum oven at 40 °C. Subsequently, the silk cocoons were placed in a home-built tubular furnace for carbonization at a 900 °C for 4 h under argon atmosphere with a heating rate of 5 °C/min. The silk-derived carbon materials activated by Co were washed with deionized water and dried at 50 °C for 24 h in a vacuum oven. The obtained products were labeled Co@NCF-A, where A denotes the concentration of $Co(NO_3)_2$ (0.4, 0.8, 1, 1.2, or 1.6 wt%). As a control, silk cocoons without Co activation were synthesized using the same procedure and were labeled NCF.

2.2. Physicochemical characterizations

Field emission transmission electron microscopy (FE-SEM, JEOL, Japan) at an acceleration voltage of 3 kV was used to observe the morphologies of all samples. Transmission electron microscopy (TEM) images were obtained by a JSM-2100 transmission electron microscope (JEOL, Japan) at an acceleration voltage of 200 kV. XRD patterns of the samples were characterized with a SIEMENS Diffraktometer at 35 kV (λ = 1.5406 Å) with a scan rate of 0.02 over the 2θ range of 10−80°. X-ray photoelectron spectra of all samples were recorded using an X-ray photoelectron spectrometer (Kratos Axis Ultra DLD) with an aluminum (mono) Kα source (1486.6 eV).

2.3. Electrochemical measurements

All electrochemical tests were performed at room temperature in a standard three-electrode system controlled by a CHI 660E electrochemistry workstation. A carbon rod and a saturated calomel electrode were used as the counter and reference electrode, respectively. In all measurements, the SCE reference electrode was calibrated with respect to the reversible hydrogen electrode ($E_{RHE} = E_{SCE} + 0.244$ V). To prepare the working electrode, all samples were fixed in a Teflon electrode clamp and immersed in 0.5 M H_2SO_4. The performance of the catalysts was recorded by linear sweep voltammetry (LSV) at a scan rate of 2 mV/s. Electrochemical impedance spectroscopy (EIS) was carried out at 0.121 V vs RHE over a frequency range from 10^{-2}−10^6 Hz. All electrochemical measurements were performed without IR compensation.

3. Results and discussion

The metallic Co nanoparticles constructed in porous silk derived carbon fibers (Co@NCFs) were synthesized by the impregnation of cobalt ions into silk fiber and pyrolysis under inert atmosphere (see Experimental section for details). Due to the strong coordination interaction between the cobalt ions and the abundant functional groups, such as amino and carboxyl groups, from silk, the cobalt ions can be easily accommodated by silk fibers. During the pyrolysis process, cobalt ions can be reduced via carbothermic reaction to metallic cobalt nanoparticles. In addition, the metallic cobalt nanoparticles can act as catalysts for the crystallization of carbon, and thin graphitized carbon layers can form on the surface of the cobalt nanoparticles, resulting in a unique core−shell structure. As a result, the metallic cobalt nanoparticles can be embedded in nitrogen-doped carbon fibers via this facile and robust host-

guest strategy. The morphology of Co@NCFs is characterized by field emission scanning electron microscopy (FE-SEM), as shown in Fig. 1a–b. For comparison, a sample without the addition of cobalt during the synthetic process was also fabricated (NCF). The silk cocoon consists of hundreds of individual fibers with diameters in the range of 10–20 μm, and the twin fibers with smooth surfaces are distributed randomly, forming a 3D network. After the carbonization at 900 °C in an Ar/NH_3 atmosphere, the organic silk fibers convert into N-doped carbonized fibers. Inheriting its morphology from silk, NCF shows a fibrous structure (~20 μm in diameter) with a relatively smooth surface (Fig. S1). In contrast, the surface of Co@NCFs becomes quite rough and porous with the introduction of cobalt (Fig. 1a and b).

The results indicate that the cobalt nanoparticles play a key role in generating the porous surface of NCFs during high-temperature pyrolysis, which will provide more active sites. The transmission electron microscopy (TEM) image shown in Fig. 1c reveals that the cobalt nanoparticles are uniformly dispersed in the porous carbon matrix. The cobalt nanoparticles are approximately 20 nm in diameter. The high-resolution TEM image further confirms that the metallic cobalt nanoparticles are surrounded by several thin layers of graphitized carbon. The lattice fringe of the cobalt nanoparticles is approximately 2.0 Å, which can be indexed to the (111) facet of metallic cobalt. The surrounding carbon also displays a lattice fringe of the (002) plane of carbon.

Fig. 2a shows the typical high angle annular dark field-scanning transmission electron microscopy (HAADF-STEM) image of Co@NCFs-II, which confirms the loading of cobalt nanoparticles tens of nanometers in diameter within the carbon matrix. This is consistent with the SEM and TEM images in Fig. 1. To gain additional insight into the elemental distribution within Co@NCFs-II, STEM-EDS mapping images were also examined and are shown in Fig. 2b–e. The mapping image displays three elements: carbon, nitrogen and cobalt. The carbon and nitrogen belong to the N-doped carbon fibers, which matched very well, verifying that the nitrogen is homogenously doped in the carbon matrix. In addition, cobalt is well matched with the white spots in Fig. 2b, confirming that the nanoparticles are indeed cobalt nanoparticles. The cobalt nanoparticles were dispersed throughout the carbon matrix, which is beneficial for the surface reaction. The corresponding line-scan STEM-EDX spectra for Co@NCF-II exhibit C, N and Co, confirming the formation of the Co@NCF-II core–shell structure. In addition, Fig. 3b display the uniformly distribution of carbon and nitrogen, indicating the successfully fabrication of N-doped carbon.

The Co@NCF-II and NCF were further characterized by X-ray diffraction (XRD), as shown in Fig. 4a. The diffraction peaks

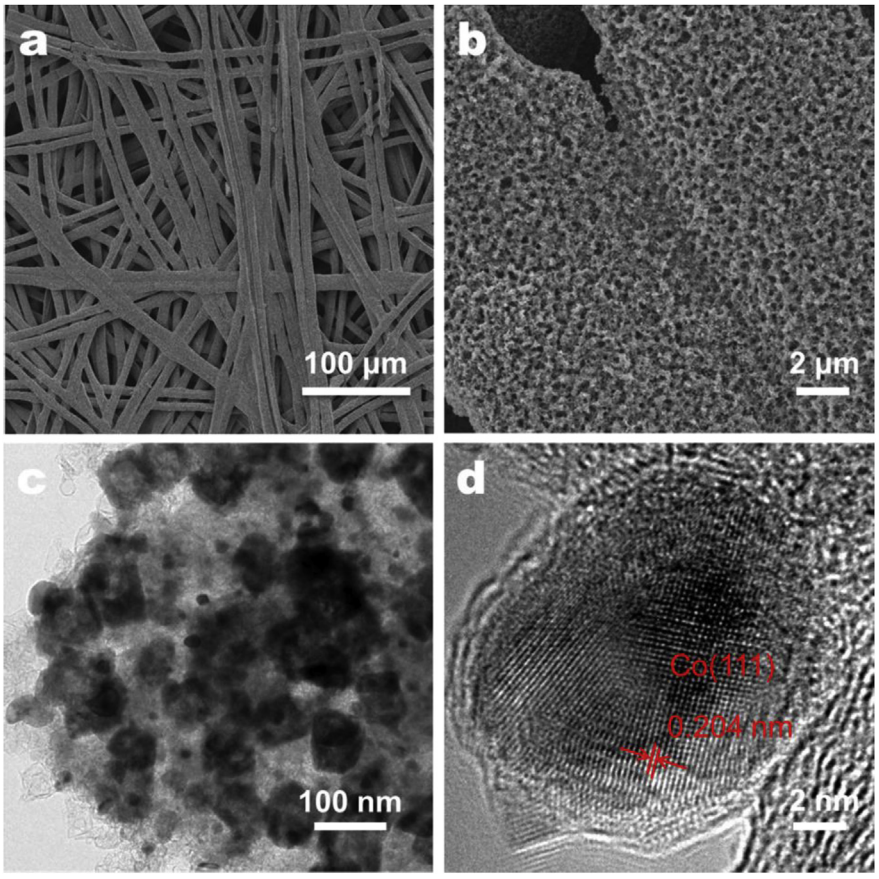

Fig. 1. (a, b) FE-SEM, (c) TEM and (d) HRTEM images of the Co@NCF-II hybrid. The concentration of $Co(NO_3)_2$ used for the preparation of Co@NCF-II is 0.8 wt%.

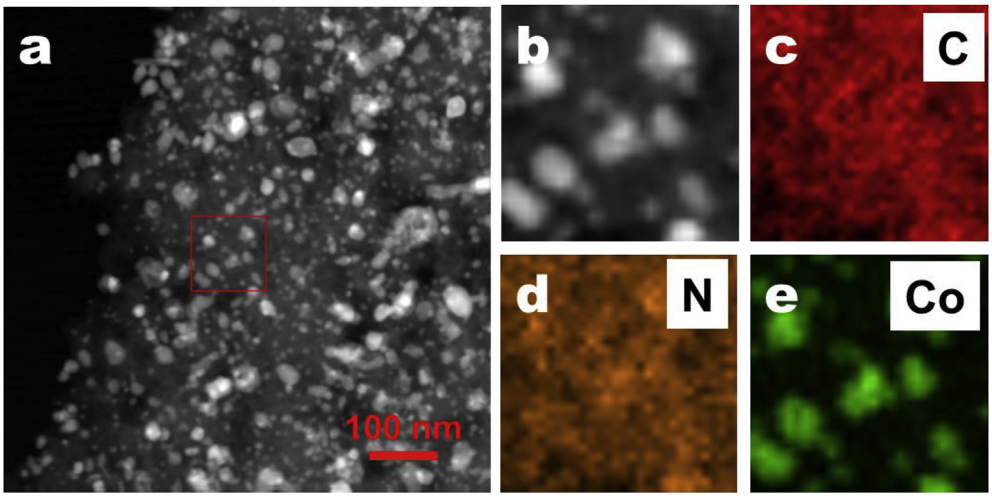

Fig. 2. (a) HAADF-STEM and (b–d) STEM-EDS mapping images of the Co@NCF-II hybrid. The concentration of $Co(NO_3)_2$ used for the preparation of Co@NCF-II is 0.8 wt%.

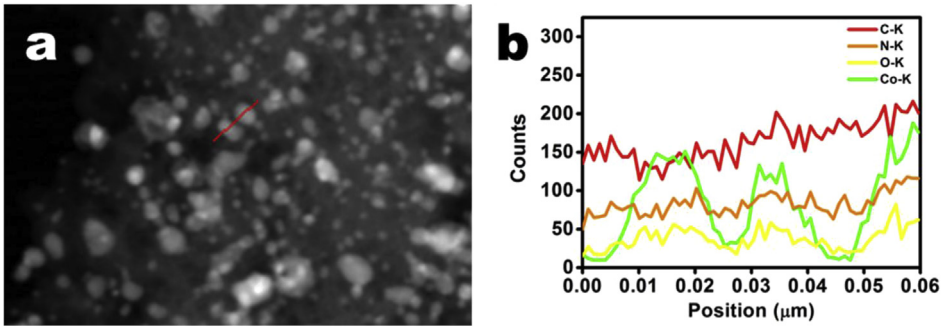

Fig. 3. (a) HAADF-STEM and (b) line scan STEM-EDS spectra of Co@NCFs. The concentration of $Co(NO_3)_2$ used for the preparation of Co@NCF is 0.8 wt%.

located around 24° for NCF are broad and weak, suggesting the partially crystalline of carbon. This indicates that after pyrolysis at the high temperature of 900 °C, the derived NCF without Co NPs still mainly consist of amorphous carbon. In contrast, the Co@NCF-II with different amounts of Co all show intense and sharp peaks, located at 26.2°, which are attributed to the (002) crystallographic plane of graphite, indicating that the graphitic structure was obtained after carbonization.

The presence of cobalt and nitrogen is further revealed by the X-ray photoelectron spectroscopy (XPS) of Co@NCF-II (Fig. 4). The XPS survey of the Co@NCF-II exhibit carbon, nitrogen, oxygen and cobalt elements, as shown in Fig. S2. In contrast to the intense O peak in NCF, the O peak in Co@NCF-II is relatively weak. This is likely due to the metallic cobalt catalyzing the graphitization of silk and the more thorough removal of oxygen species. The high resolution C 1 s spectrum for NCF is shown in Fig. 4b, the spectrum of NCF are fitted into four peaks with binding energies at nearly 284.5 (−C−C/H), 285.1 (−C−N), 286.3 (C−OH/C−N) and 292.8 eV (−O═C−N) [33]. Similarly, the C 1s spectrum of Co@NCF-II also exhibit four peaks located at 284.6, 285.1, 286.1 and 291.1 eV, respectively.

Silk fiber is a filamentous natural protein fiber made of repeated amino acid patterns [33,34]. In addition, silk fibers have a wealth of polypeptides and a high content of C, N, and O elements, which might provide a great opportunity for conversion into naturally derived heteroatom doped carbon catalysts. Fig. 4d displays the N 1s spectra of the NCF. The N 1s spectrum can be deconvoluted into three peaks centered at 397.4, 399.1, and 400.3, which are consistent with pyridinc (N-5), pyrrolic (N-6), and graphitic (N-Q), respectively, indicating that the nitrogen in amino group has transformed into N-5, N-6 and N-Q during the carbonization process. The N 1s spectra of the Co@NCF-II also exhibit three peaks with binding energies at 397.5, 399.8 and 401.1 eV, respectively. The valance states of cobalt in Co@NCF-II can be determined by the Co 2p spectrum after deconvolution, two core-level peaks located at ~780 eV and 796 eV are attributed to Co $2p_{1/2}$ and $2p_{3/2}$, respectively. The peak at approximately 778.5 eV can be attributed to metallic cobalt. Meanwhile, peaks for Co (II) are also detectable, which may be caused by the partially surface oxidation of metallic cobalt. The binding states of nitrogen were also revealed in the N 1s spectrum. All of these observations manifest that metallic cobalt nanoparticles embedded in N-doped carbon fibers were prepared successfully through the host-guest strategy.

Fig. 5 shows the morphologies of the Co@NCF with different Co precursor concentrations (0.4, 1, 1.2, or 1.6 wt%).

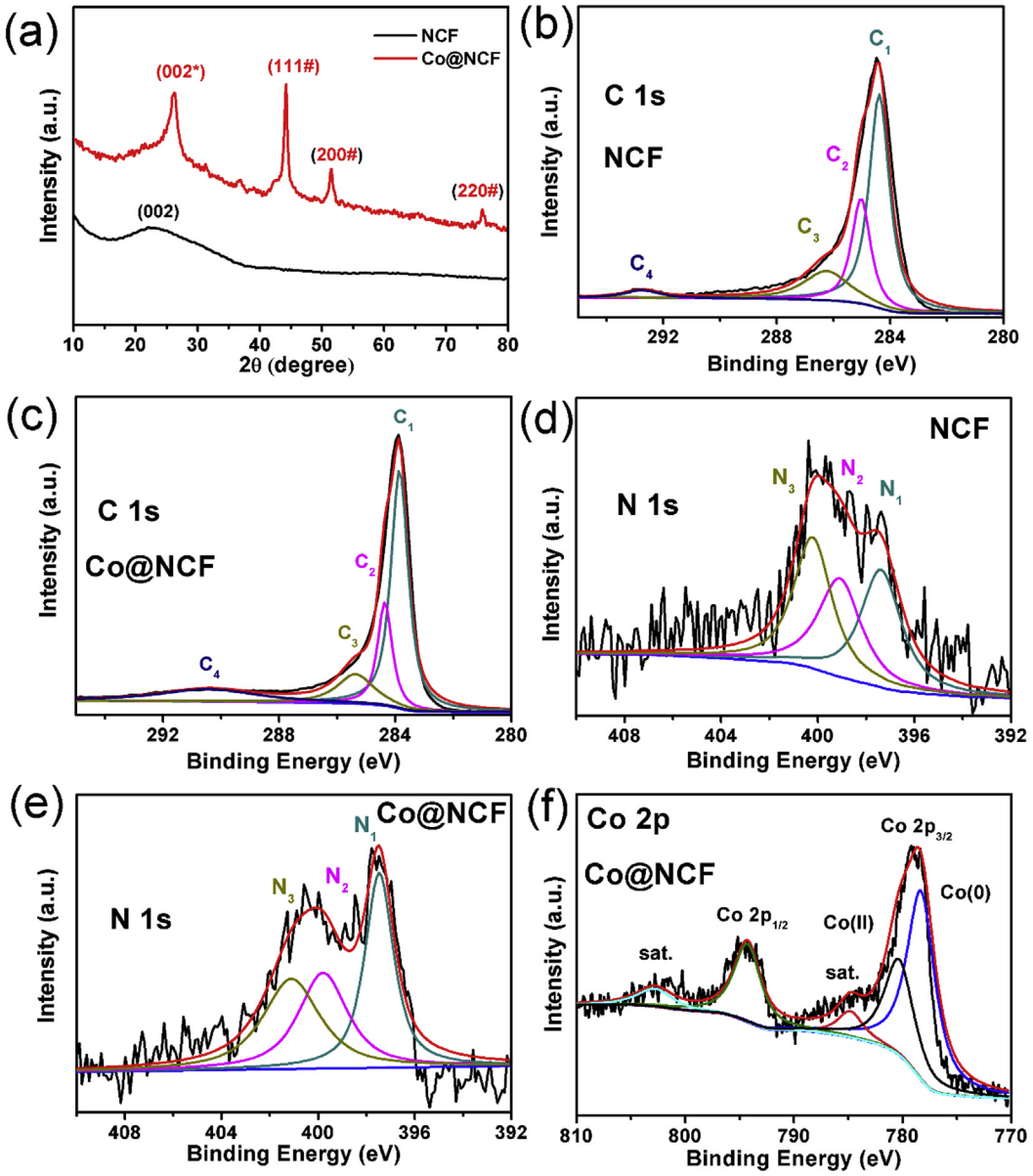

Fig. 4. (a) XRD patterns of the NCF and Co@NCF-II. C 1s XPS spectra of the (b) NCF and (c) Co@NCF. N 1s XPS spectra of the (d) NCF and (e) Co@NCF-II. (f) Co 2p XPS spectra of the Co@NCF-II. The concentration of $Co(NO_3)_2$ used for the preparation of Co@NCF-II is 0.8 wt%.

The samples are labeled as Co@NCF-I, Co@NCF-III, Co@NCF-IV and Co@NCF-V accordingly. The morphologies of Co@NCF-II prepared by the Co precursor of 0.8 wt% are shown in Figs. 1−3. As shown in Fig. 5, with increased Co precursor concentration, the density of the Co NPs in the NCF increased along with the increased size. At the precursor concentration of 0.4 and 0.8 wt%, the Co NPs can still individually exist in the NCF with seriously aggregated particles. However, when the precursor concentration increased to 1, 1.2 and 1.6 wt%, the size of the Co NPs became larger, and the Co NPs gathered together side by side, as shown in Fig. 5e−h.

Meanwhile, the XRD pattern of the Co@NCFs with different contents are shown in Fig. 6a. At relative lower Co precursor concentrations (0.4−1 wt%), the Co@NCF-I and Co@NCF-II exhibit four peaks located at 26.2°, 44.1°, 51.4° and 75.7°, respectively, corresponding to the (002) planes of graphite carbon, the (111), (200) and (220) planes of metallic cobalt. It demonstrated the successful reduction of cobalt ions to the metallic state during carbonization. When the Co precursor concentration increased to 1, 1.2 and 1.6 wt%, the XRD patterns of the Co@NCF-III, Co@NCF-IV and Co@NCF-V display the CoO phase with peaks at 36.7° and 42.5°, indicating the partial oxidation of metallic Co due to the high Co content.

The Co 2p XPS spectra of the Co@NCF with different Co contents also demonstrate that the relative high loading of Co NPs in NCF would lead to the partially surface oxidation, resulting in the passivation for the electrocatalytic activity. Table 1 summarizes the XPS atomic concentrations of the Co, N and O in Co@NCF hybrid with different Co contents. The oxygen concentration increased sharply with the increased Co concentration.

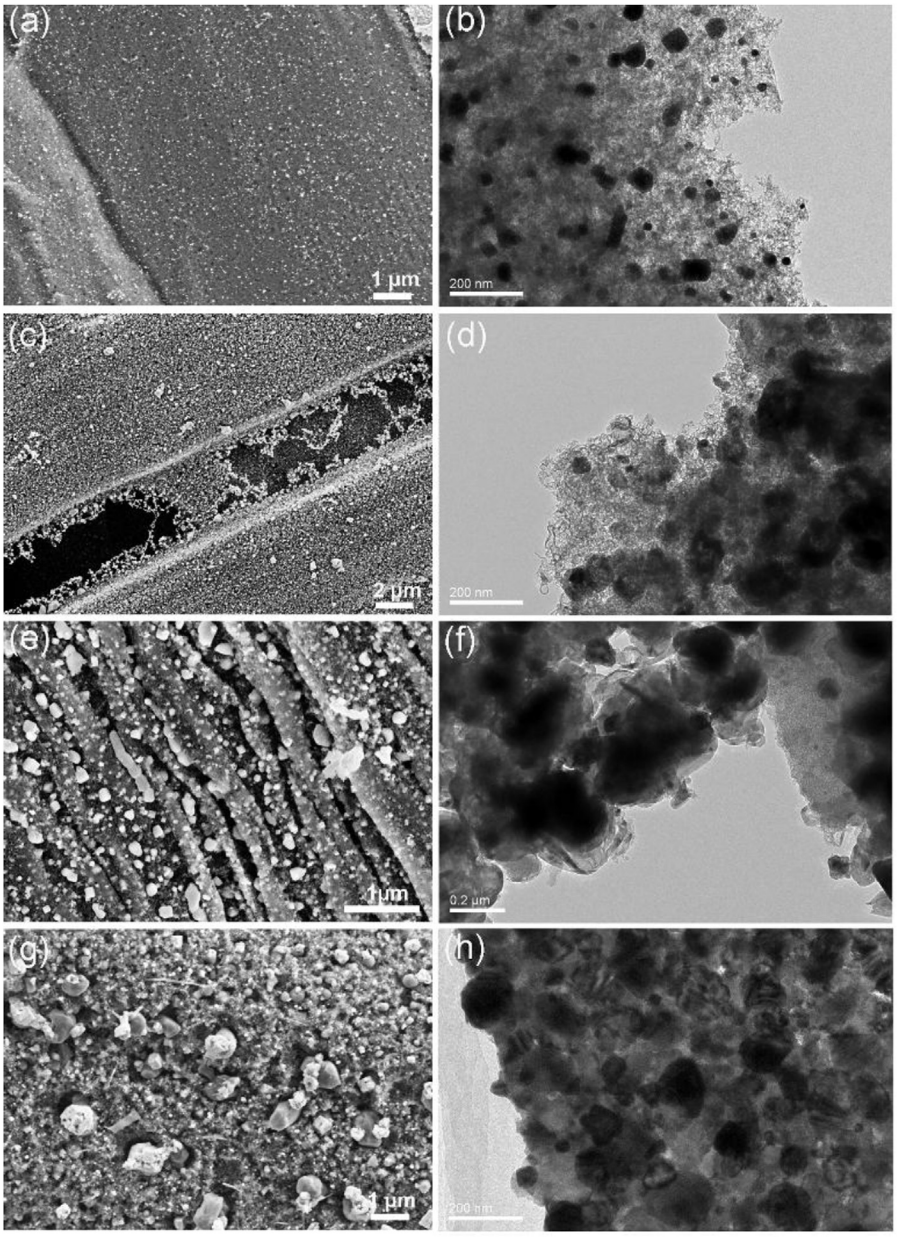

Fig. 5. TEM and FE-SEM images of the Co@NCF with different Co precursor concentrations (0.4, 1, 1.2, or 1.6 wt%). The samples are labeled as (a, b) Co@NCF-I, (c, d) Co@NCF-III, (e, f) Co@NCF-IV, (g, h) Co@NCF-V accordingly.

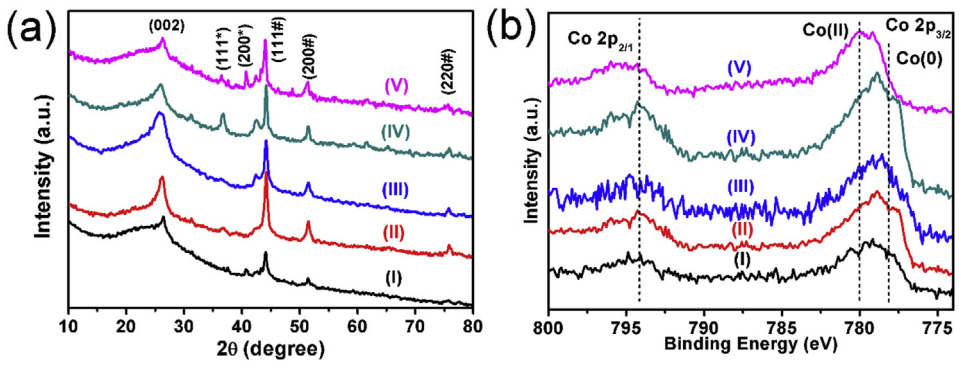

Fig. 6. (a) XRD patterns and (b) Co 2p XPS spectra of the Co@NCF with increased Co contents from (I) to (V).

Table 1
XPS atomic concentrations of the Co, N and O in Co@NCF hybrid with different Co contents.

Samles	Co atomic concentrations (%)	N atomic concentrations (%)	O atomic concentrations (%)
Co@NCF-I	0.61	4.33	4.68
Co@NCF-II	0.97	3.62	4.85
Co@NCF-III	1.30	3.25	5.63
Co@NCF-IV	1.43	3.46	8.58
Co@NCF-V	1.54	4.05	10.57

The electrochemical HER performances of Co@NCFs with different Co contents were evaluated using a standard three-electrode system in 0.5 M H_2SO_4. For comparison, the polarization curves for NCFs and commercial 20% Pt/C were also collected. The Co@NCF and NCF were directly used as the electrode. For the control of the geometric area of the working electrode, we cut the fibers into regular piece (1 × 1 cm × cm) (Fig. S3). As shown in Fig. 7a and b, the NCFs electrode without metallic cobalt shows relatively high overpotential for HER, suggesting its weak activity. In contrast to the cooperation of metallic cobalt, the Co@NCFs-II manifest significantly enhanced HER performance. The Co@NCF-II shows the lowest overpotential among the Co@NCFs, revealing the best HER activity. Table 2 summarizes the overpotentials of the various Co@NCF electrocatalysts with different Co contents, NCF and commercial 20% Pt/C at a current density of 10 mA/cm^2. The NCFs prepared without cobalt shows an overpotential of approximately 320 mV, while the Co@NCFs show significantly lower overpotentials.

The lowest overpotential at 10 mA/cm^2 is 61 mV for Co@NCF-II, comparable with commercial 20% Pt/C, which is among one of the best cobalt-based HER electrocatalysts [30,31]. In addition, at an overpotential of 200 mV, the Co@NCF-II electrode shows the highest current density (83.77 mA/cm^2), which is approximately 55.8 times larger than that of NCFs (1.55 mA/cm^2). To gain more insight into the HER

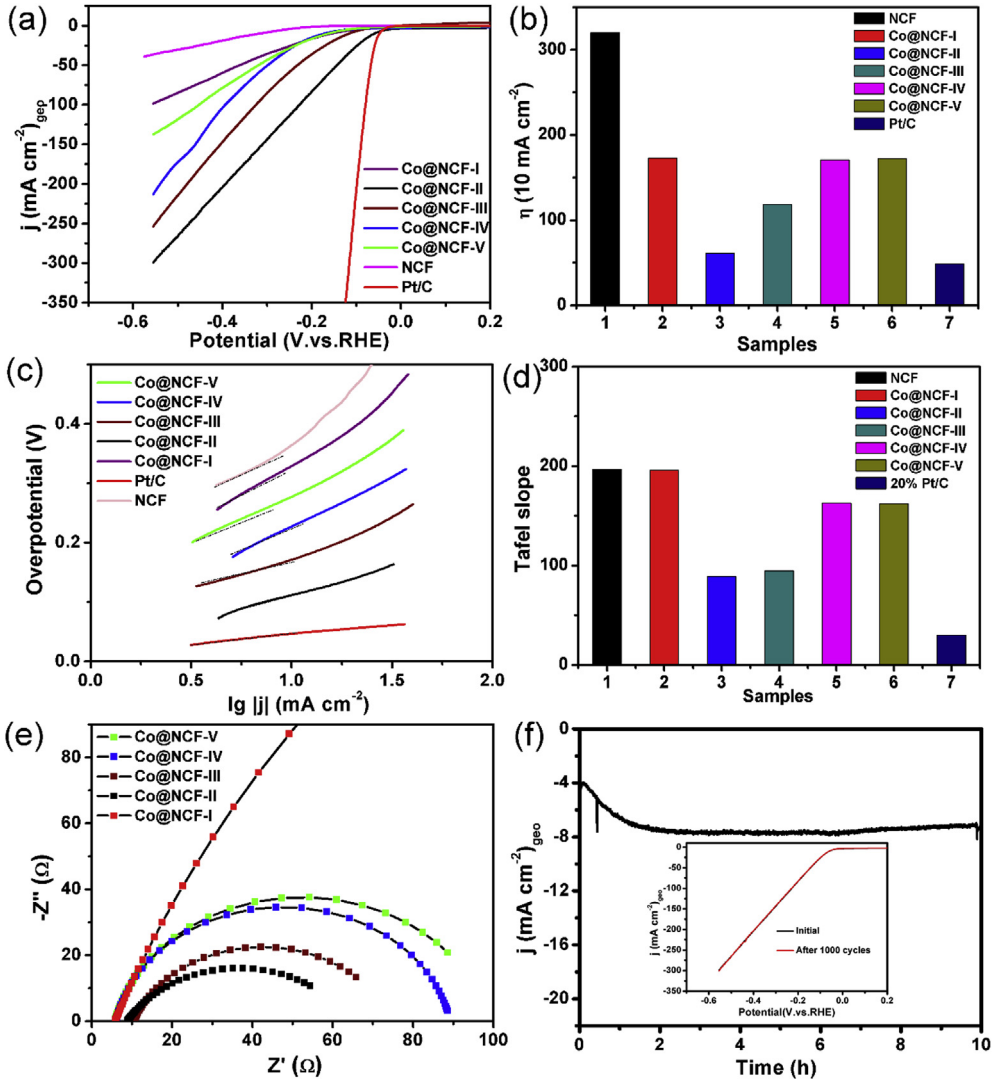

Fig. 7. (a) Polarization curves, (b) overpotential at 10 mA/cm^2, (c) Tafel plots, (d) Tafel slopes and (e) Nyquist plots of Co@NCF with different Co contents in N_2-saturated 0.5 M H_2SO_4. (d) Time dependence of the current density for Co@NCF-II. The potential is −0.3 V for the chronoamperometry test. Inset in Fig. 7f is the polarization curves of the Co@NCF-II before and after 1000 cycles.

Table 2
Electrochemical performance of Co@NCFs, NCF and 20% Pt/C.

Samples	η[a]	j[b]	Tafel slope[c]	R_{ct}[d]
NCF	320	1.55	197	NM[e]
Co@NCF-I (0.4 wt%)	173	16.62	196	550
Co@NCF-II (0.8 wt%)	61	83.77	89	64
Co@NCF-III (1 wt%)	118	36.19	95	73
Co@NCF-IV (1.2 wt%)	171	17.25	163	91
Co@NCF-V (1.6 wt%)	172	16.83	162	102
20% Pt/C	49	NM	30	NM

[a] Overpotential at 10 mA/cm^2 (mV).
[b] Current density at η = 200 mV (mA/cm^2).
[c] (mV/dec).
[d] Charge transfer resistance (Ω).
[e] Not measured.

performance, the Tafel plots of different samples were also investigated. The Co@NCF-II electrocatalysts show a low Tafel slope of 89 mV/dec, which is much smaller than that of NCF (196 mV/dec) (Fig. 7c and d). The results imply that faster HER kinetics can be achieved by adjusting the amount of cobalt. To gain a deeper understanding of the superior activity of Co@NCF-II, electrochemical impedance spectroscopy (EIS) analysis was performed (Fig. 7e). Co@NCF-0.8 has the lowest charge transfer resistance, indicating its faster charge transport kinetics. The LSV, Tafel slope and EIS results all indicate that with an increased amount of Co, the HER activity is first enhanced and then decreased when the mass ratio of Co to NCF reaches 1%. This is a result of the excess amount of metallic Co in the NCFs leading to Co oxide formation in the NCFs, which was detected by the XRD and XPS results. The formation of Co oxides would result in a decrease in HER activity. By adjusting the synthetic conditions, the as-synthesized Co@NCF-II is almost purely metallic-phase Co, as verified by the XRD results (Figs. 4a and 6a).

Asides from the HER activity, the durability is another crucial factor to evaluate a good electrocatalyst. The time dependence of the current density curve was obtained to evaluate the durability of Co@NCF-II. As is illustrated in Fig. 7f, there was no significant decrease in the current density during continuous electrolysis over several hours, verifying its good stability. The inset in Fig. 7f shows the polarization curves of the Co@NCF-II before and after 1000 cycles and it has negligible decrease. The morphology of Co@NCF-II after stability tests are shown in Fig. S4. There are large amount of Co NPs exist in the NCF, indicating the superior stability of Co NP protected by NCF. The superior HER activity and good stability of Co@NCF-II make it one of the most promising HER electrocatalysts for large-scale application.

According to the above results, the superior activity and good stability of Co@NCF-II can be attributed to the synergistic interplay of the metallic cobalt nanoparticles and the N-doped carbon fibers. First, the one-dimensional fibrous structure inherited from silk greatly facilitates surface reactions, resulting in faster reaction kinetics. Second, with the introduction of cobalt, the surfaces of Co@NCFs become more rough and more porous, which leads to more exposed active site and accelerates the HER rates. Lastly, but most importantly, due to the host-guest interaction between cobalt and silk, the metallic cobalt nanoparticles were surrounded by thin layers of graphitized carbon with homogenous N-doping by a robust and eco-friendly procedure. On one hand, the thin graphitized carbon layers strongly promote electron penetration from the metallic cobalt nanoparticles to the graphitized carbon surface. The electron density on graphitized carbon can be increased by N-doping, which results in superior HER activity [28]. On the other hand, the carbon layers can fix the metallic cobalt nanoparticles into the carbon matrix to avoid aggregations and protect them from corrosion in acid, which is beneficial for good HER stability.

4. Conclusion

In summary, we have demonstrated a host-guest approach to fabricate metallic cobalt embedded in N-doped carbon fibers using cobalt and natural silk as precursors. These materials can serve as some of the most promising HER electrocatalysts. The electrochemical results reveal that the Co@NCFs display comparable activity with commercial 20% Pt/C, as well as good stability. The high HER performance of Co@NCFs can be attributed to the host-guest interaction and the synergistic interplay of the metallic cobalt nanoparticles and the N-doped carbon fibers. These findings provide a novel and unique route to exploring high-performance noble-metal-free HER electrocatalysts in a facile, robust and eco-friendly manner. This host-guest strategy can be easily adapted to fabricate other transition-metal-embedded N-doped carbon fibers for versatile electrochemical applications.

Conflict of interest

The authors declare no conflict of interest.

Acknowledgment

This study was supported by the National Natural Science Foundation of China (NSFC) (Grant No. 21203137, 51573166) and the Natural Science Foundation of Zhejiang Province (Grant No. LQ16E020005).

Appendix A. Supplementary data

Supplementary data related to this article can be found at http://dx.doi.org/10.1016/j.gee.2017.01.007.

References

[1] N.S. Lewis, D.G. Nocera, Proc. Natl. Acad. Sci. 103 (2006) 15729–15735.
[2] J.A. Turner, Science 305 (2004) 972–974.
[3] W.T. Hong, M. Risch, K.A. Stoerzinger, A. Grimaud, J. Suntivich, S.H. Yang, Energy Environ. Sci. 8 (2015) 1404–1427.
[4] M.S. Faber, S. Jin, Energy Environ. Sci. 7 (2014) 3519–3542.
[5] Y. Jiao, Y. Zheng, M. Jaroniec, S.Z. Qiao, Chem. Soc. Rev. 44 (2015) 2060–2086.

[6] J. Duan, S. Chen, B.A. Chambers, G.G. Andersson, S.Z. Qiao, Adv. Mater. 27 (2015) 4234–4241.
[7] L. Yu, B.Y. Xia, X. Wang, X.W. Lou, Adv. Mater. 28 (2016) 92–97.
[8] F.X. Ma, H.B. Wu, B.Y. Xia, C.Y. Xu, X.W. Lou, Angew. Chem. Int. Ed. 54 (2015) 15395–15399.
[9] L. Liao, S. Wang, J. Xiao, X. Bian, Y. Zhang, M.D. Scanlon, X. Hu, Y. Tang, B. Liu, H.H. Girault, Energy Environ. Sci. 7 (2014) 387–392.
[10] X.D. Wang, Y.F. Xu, H.S. Rao, W.J. Xu, H.Y. Chen, W.X. Zhang, D.B. Kuang, C.Y. Su, Energy Environ. Sci. 9 (2016) 1468–1475.
[11] J. Zhang, T. Wang, P. Liu, S. Liu, R. Dong, X. Zhuang, M. Chen, X. Feng, Energy Environ. Sci. 9 (2016) 2789–2793.
[12] M. Zou, J. Chen, L. Xiao, H. Zhu, T. Yang, M. Zhang, M. Du, J. Mater. Chem. A 3 (2015) 18090–18097.
[13] M. Zou, J. Zhang, H. Zhu, M. Du, Q. Wang, M. Zhang, X. Zhang, J. Mater. Chem. A 3 (2015) 12149–12153.
[14] H.B. Wu, B.Y. Xia, L. Yu, X.-Y. Yu, X.W. Lou, Nat. Commun. 6 (2015) 6512.
[15] J. Duan, S. Chen, M. Jaroniec, S.Z. Qiao, ACS Nano 9 (2015) 931–940.
[16] Y. Zheng, Y. Jiao, Y. Zhu, L.H. Li, Y. Han, Y. Chen, A. Du, M. Jaroniec, S.Z. Qiao, Nat. Commun. 5 (2014) 3783.
[17] Y. Jiao, Y. Zheng, K. Davey, S.Z. Qiao, Nat. Energy 1 (2016) 16130.
[18] H. Zhu, J. Zhang, R. Yanzhang, M. Du, Q. Wang, G. Gao, J. Wu, G. Wu, M. Zhang, B. Liu, J. Yao, X. Zhang, Adv. Mater. 27 (2015) 4752–4759.
[19] S. Peng, L. Li, X. Han, W. Sun, M. Srinivasan, S.G. Mhaisalkar, F. Cheng, Q. Yan, J. Chen, S. Ramakrishna, Angew. Chem. Int. Ed. 126 (2014) 12802–12807.
[20] M.S. Faber, R. Dziedzic, M.A. Lukowski, N.S. Kaiser, Q. Ding, S. Jin, J. Am. Chem. Soc. 136 (2014) 10053–10061.
[21] J. Staszak-Jirkovsky, C.D. Malliakas, P.P. Lopes, N. Danilovic, S.S. Kota, K.-C. Chang, B. Genorio, D. Strmcnik, V.R. Stamenkovic, M.G. Kanatzidis, N.M. Markovic, Nat. Mater. 15 (2016) 197–203.
[22] Y. Sun, C. Liu, D.C. Grauer, J. Yano, J.R. Long, P. Yang, C.J. Chang, J. Am. Chem. Soc. 135 (2013) 17699–17702.
[23] Z. Pu, Q. Liu, P. Jiang, A.M. Asiri, A.Y. Obaid, X. Sun, Chem. Mater. 26 (2014) 4326–4329.
[24] X. Li, Y. Fang, F. Li, M. Tian, X. Long, J. Jin, J. Ma, J. Mater. Chem. A 4 (2016) 15501–15510.
[25] X. Zhong, Y. Jiang, X. Chen, L. Wang, G. Zhuang, X. Li, J.G. Wang, J. Mater. Chem. A 4 (2016) 10575–10584.
[26] X. Yang, A.Y. Lu, Y. Zhu, M.N. Hedhili, S. Min, K.W. Huang, Y. Han, L.J. Li, Nano Energy 15 (2015) 634–641.
[27] Y. Hou, Z. Wen, S. Cui, S. Ci, S. Mao, J. Chen, Adv. Funct. Mater. 25 (2015) 872–882.
[28] J. Deng, P. Ren, D. Deng, X. Bao, Angew. Chem. Int. Ed. 54 (2015) 2100–2104.
[29] W. Zhou, J. Zhou, Y. Zhou, J. Lu, K. Zhou, L. Yang, Z. Tang, L. Li, S. Chen, Chem. Mater. 27 (2015) 2026–2032.
[30] X. Zou, X. Huang, A. Goswami, R. Silva, B.R. Sathe, E. Mikmeková, T. Asefa, Angew. Chem. Int. Ed. 126 (2014) 4461–4465.
[31] H. Jin, J. Wang, D. Su, Z. Wei, Z. Pang, Y. Wang, J. Am. Chem. Soc. 137 (2015) 2688–2694.
[32] Z.L. Wang, X.F. Hao, Z. Jiang, X.P. Sun, D. Xu, J. Wang, X.B. Zhang, J. Am. Chem. Soc. 137 (2015) 15070–15073.
[33] Q. Wang, R. Yanzhang, X. Ren, H. Zhu, M. Zhang, M. Du, Int. J. Hydrogen Energy 41 (2016) 21870–21882.
[34] Q. Wang, R. Yanzhang, Y. Wu, H. Zhu, J. Zhang, M. Du, X. Liang, RSC Adv. 6 (2016) 34219–34224.